2009

Optically Resonant Nanophotonic Devices for Label-Free Biomolecular Detection

Julie M. Goddard, *University of Massachusetts - Amherst*
S. Mandal
D. Erickson

Chapter 16
Optically Resonant Nanophotonic Devices for Label-Free Biomolecular Detection

Julie Goddard, Sudeep Mandal, and David Erickson

Abstract Optical devices, such as surface plasmon resonance chips and waveguide-based Mach–Zehnder interferometers, have long been successfully used as label-free biomolecular sensors. Recently, however, there has been increased interest in developing new approaches to biomolecular detection that can improve on the limit of detection, specificity, and multiplexibility of these early devices and address emerging challenges in pathogen detection, disease diagnosis, and drug discovery. As we describe in this chapter, planar optically resonant nanophotonic devices (such as ring resonators, whispering gallery modes, and photonic crystal cavities) are one method that shows promise in significantly advancing the technology. Here we first provide a short review of these devices focusing on a handful of approaches illustrative of the state of the art. We then frame the major challenge to improving the technology as being the ability to provide simultaneously spatial localization of the electromagnetic energy and biomolecular binding events. We then introduce our "Nanoscale Optofluidic Sensor Arrays" which represents our approach to addressing this challenge. It is demonstrated how these devices serve to enable multiplexed detection while localizing the electromagnetic energy to a volume as small as a cubic wavelength. Challenges involved in the targeted immobilization of biomolecules over such a small area are discussed and our solutions presented. In general, we have tried to write this chapter with the novice in mind, providing details on the fabrication and immobilization methods that we have used and how one might adapt our approach to their designs.

D. Erickson (✉)
Sibley School of Mechanical and Aerospace Engineering, Cornell University, Ithaca, NY 14853, USA
e-mail: de54@cornell.edu

X. Fan (ed.), *Advanced Photonic Structures for Biological and Chemical Detection*, Integrated Analytical Systems,
DOI 10.1007/978-0-387-98063-8_16,

16.1 Introduction

The global market for biosensors and bioelectronics has grown from $6.1 billion in 2004 to an expected $8.2 billion in 2009 (roughly the time of the publication of this book) with approximately 40% of this representing demand within USA. Within this larger market optical sensors and biosensors are expected to grow the fastest with the large medical/diagnostic market continuing to offer the best opportunities (note that the above figures are compiled from a variety of commercially available market surveys that I will not specifically reference here). Readers interested in details of existing commercially available optical biosensors and application areas are suggested to consult a recent review paper by Rich and Myszka[1], who provide an excellent survey of the 2006 literature.

This enlarged interest is largely driven by recent advancements in proteomics and genomics, which have yielded a larger number of more specific biomarkers that can be associated with specific disease states[2–5] and pharmacological responses.[6] Point-of-care sensing platforms that can detect these biomarkers at very low concentrations among an enormous number of background interferants in a blood or saliva sample could lead to earlier stage diagnosis of complex diseases like cancer[7–10]. The second broad application area relates to the growing need for military, government, and other civilian organizations to be able to rapidly detect and identify pathogenic threats. The detection of water-[11], food-[12], or air-borne bacterial pathogens[13,14] requires devices with high sensitivity and specificity but introduce other engineering challenges such as larger sample volumes to be processed and often more complex background media. While greater sensitivity leading to earlier detection is critical, it is perhaps more important to minimize false alarm rates since the economic and social consequences of a detection event can be significant. Viral detection adds further complications to detection platforms in that they must be able to account for high rates of mutagenic drift and therefore detect what amounts to a moving target.

16.1.1 A Brief Overview of Biomolecular Detection

Though much of this book covers various methods of biomolecular detection and thus it can be assumed that the reader has a certain familiarity with the concept, we thought we would begin this chapter with a high-level overview of the different methods to help place our work in context. Uninterested readers can skip ahead to Sect. 16.1.2. In the most general sense, there are two ways in which a biomolecular detection reaction can be carried out. The first is homogeneously, where both the target (e.g., a blood-borne antibody created by the immune system in response to the presence of a tumor) and probe (e.g., an antigen that will specifically bind to the target antibody) are dispersed in the solution phase. Binding between the probe and the target is detected by observing changes in bulk solution properties such as

optical absorbance, fluorescence, or electrical conductivity. Quantification is typically done then by relating the change in the interrogated bulk property to the concentration of target in the sample through a predetermined calibration curve. If no change is detected the target concentration is said to be below the limit of detection (LOD). The slope of this calibration curve is referred to as the "internal sensitivity" (see Erickson et al.[15] for more details on the use of these terms). The advantage of homogeneous techniques is that they tend to have higher overall reaction rates since both the target and probe are mobile in solution and therefore often the time required for analysis is lower. Additionally since all the chemistry is carried out in solution, the overall detection reaction can be easier to conduct and may be more robust. The major disadvantage of homogeneous reactions is that they are much harder to multiplex since binding is not spatially localized within the reaction volume. To increase the parallelity of such reactions, it is common to use either arrays of tiny reaction wells (such as is done in 96 or 384 well plates) or to spectrally multiplex using, for example, fluorescent tags that emit at different colors.

Heterogeneous detection reactions involve first immobilizing a probe on a surface and then introducing the test sample to the surface. The presence of a target is determined by observing changes in a particular surface property (e.g., fluorescence, refractive index, or mechanical compliance). Heterogeneous reactions are much easier to multiplex since the probes and detection signal can be spatially localized. They can also have fundamentally greater limits of detection since one is essentially concentrating the detected analyte from a dispersed 3D phase to a 2D one. The disadvantage is that the analysis time can be longer since the targets must diffuse to the probe site. The incorporation of microfluidic elements to confine the targets closer to the surface (thereby decreasing the diffusion distance) can help to mitigate this problem.

Heterogeneous detection reactions are commonly further subdivided into what are known as labeled or label-free techniques. Labeled techniques are those that require at least one more reaction step, either prior to or after the probe–target reaction, to attach a secondary molecule to the probe that can be more easily detected than the reaction itself. The most commonly used labels are fluorescent tags (as is done in most modern nucleic acid and immunological microarrays) though other tags such as nanoparticles and radiolabels can also be used. Though the sensitivity and specificity of labeled detection can be very high (particularly if the label is also specific to the target), the added complexity of the labeling step is often undesired for point-of-care, portable, or rapid result diagnostic/detection applications. Label-free techniques seek to eliminate this secondary step and exploit some intrinsic changes in surface properties caused by the binding of the target to the surface immobilized probe. Techniques for accomplishing this are classified by the sensor transduction mechanism as either electrical, mechanical, or optical. We have discussed the advantages and disadvantages of these different modalities in a recent review paper[15] and so will not go into in detail here. Briefly, however, mechanical techniques rely on detecting changes in the mechanical behavior of a surface due to the accumulation of mass on it. This can manifest

itself in either a change in the natural frequency of a cantilever or membrane, additional surface stress induced by electrostatic repulsion/attraction between bound molecules, or changes in the transmission properties of surface guided acoustic waves. Electrical techniques sense changes in surface conductivity or capacitance due to the accumulation of charged molecules. Since often only an impedance measurement is required, electrical methods represent likely the simplest transduction mechanism but they have additional complications such as sensitivity to background electrolytes and relatively complex device fabrication.

16.1.2 Advantages of Label-Free Optical and Nanotechnological Techniques

Optical techniques represent perhaps the most pervasive method of label-free biomolecular detection. Though a number of different properties can be probed, the most common methods look for changes in the local refractive index near the surface as the amount of bound molecules increases. The primary advantages of optical techniques over analogous mechanical or electrical label-free methods are the relative ease with which devices can be fabricated and the broad range of fluids and environments in which they can be used (e.g., gas, water, and serum). Though numerous different architectures have been developed, surface plasmon resonance (SPR) biosensors have been the most commercially successful to date due to their inherently high sensitivity and lack of any complex assembly or fabrication steps. There is also considerable knowledge in the use of SPR including the extraction of kinetic data, which presents a more robust picture than might be available with a simple qualitative test. The serial nature of the traditional SPR approach, however, has proved to be a limitation of the technology in the past, though the advent of SPR-imaging techniques will likely help to resolve this.

As mentioned above, one of the major strengths of heterogeneous array-based technologies is in their ability to provide very high degrees of multiplexing. In general, however, the relatively low sensitivity of such approaches limits the types of targets, which can be reasonably expected to be interrogated, and places stricter requirements on the amount of sample processing and detection infrastructure that is required. Emerging nanotechnologies such as nanoparticles[16], nanowires and nanotubes[17,18], nanomechanical resonators[19], and (as will be discussed primarily here) nanophotonics[20–22] are of interest largely to address this failing. While many of these devices tend not to have much greater internal sensitivity (i.e., slope of the sensor response curve in response to changes in bulk properties such as conductivity or refractive index) than traditional techniques, their inherent advantage is that the total surface area or volume that is probed tends to be much smaller. As a result, the total mass required to impart a measurable transduction signal is significantly lower and therefore the potential for greatly improved LOD is significant. In general, however, the extension of these technologies to the extreme parallelity of the 2D microarray format

is complicated by the challenges involved in functionalization of individual sensor and 2D optical or electrical addressing of reaction sites with submicrometer spacing.

16.1.3 Overview of This Chapter

The goal of this chapter will be to provide an overview of the use of planar, optically resonant nanophotonic devices for biomolecular detection. Nanophotonics[23,24] represents the fusion of nanotechnology with optics and thus it is proposed that sensors based on this technology can combine the advantages of each as discussed above. Although many of the issues are the same, we focus here on optical resonance rather than plasmonic resonance (such as is used in emerging local SPR and surface-enhanced Raman spectroscopy-based biosensors).

In Sect. 16.2, we present a noncomprehensive overview of the state of the art in nanophotonic approaches to biomolecular detection. The goal of this section will be to provide sufficient background to place our work in the context, rather than providing an exhaustive review of the current literature. Following this, we attempt to take a high-level overview of the field and propose a series of overall challenges for advancing it. Sections 16.4 and 16.5 describe some of our general approaches to solve these challenges, namely, the development of nanoscale optofluidic sensor arrays (NOSA) and techniques for targeted immobilization of probes within optical cavities.

16.2 Review of Nanophotonic Devices for Biomolecular Detection

16.2.1 Brief Overview of Evanescent Field-Based Optical Sensing

While most of the optical energy is confined within the structure itself, solid-core dielectric waveguides have an exponentially decaying tail of the guided optical mode, referred to as the evanescent field, that impinges a small distance (typically on the order of the wavelength of light) into the surrounding medium. Binding of a target at a probe site within this evanescent field causes a change in the local refractive index in that region, imparting a slight phase shift to the propagating optical mode. Likely the simplest way to detect this phase shift is through interferometry with the simplest practical on-chip implementation useful for biosensing being the Mach–Zehnder interferometer (MZI) (see Refs.25–27). These designs typically consist of an input optical waveguide, which is split into two arms of equal length and then recombined to form the output optical waveguide. A section of one of these arms, called the sensing arm, is functionalized with the desired probe agent. The second arm is referred to as the reference arm and is generally left without

modification. In the absence of any surface modifications to either of the arms, the light recombining at the output port remains in phase, giving rise to constructive interference and maximal light intensity at the output port. When binding occurs at the surface of the sensing arm, it changes the local refractive index and the resulting phase shift causes the output power to drop due to destructive interference effects. An analogous approach using a Young's interferometer is discussed in Chap. 10.

16.2.2 Microring Resonators

The drawback of traditional devices such as the interferometers discussed above is that the interaction length between the optical field and the binding sites necessary for producing detectable phase shifts can be very large, often in the order of a centimeter. The major disadvantage of this is that it therefore requires a relatively large amount of actual bound mass to make an appreciable change in the transduction signal. Therefore, while the sensitivity to bulk properties, such as refractive index or mass per unit area, can be quite high, the response to absolute measures, like bound mass, tends to be relatively low (in comparison with some of the technologies to be discussed below).

Microring resonators consist of a ring waveguide adjacent to a bus waveguide. Light from a laser travels down a bus waveguide and evanescently couples into the ring resonator. When the optical path length around the ring is equal to an exact multiple of the wavelength of the excitation light, the conditions for constructive interference are met and the ring is said to be on-resonance. Under such conditions, the intensity of the light will build up in the rings until such a time as the intrinsic losses are equivalent to the input power. By exciting the bus waveguide with a tunable laser or broadband source, these resonance conditions can be detected at the output end of the bus waveguide as sharp dips in transmission. Binding events along the surface of the microring increase the refractive index in the evanescent field, effectively optically lengthening the ring and causing the resonant dips to red shift to longer wavelengths. The shift in the resonant wavelength can be related to the amount of bound mass on the surface, which in turn can be related to the solution phase concentration by empirical calibration. The degree to which this energy is trapped within the ring is reflected in a quantity called the Q-factor with higher Qs leading to greater intensity trapped in the ring (to be precise, the definition of the Q-factor is the ratio of the energy stored to the amount of energy lost in a round trip).

As an example of such a device, Chao et al.[28] demonstrated polymer microring resonators of 45mm radius having a Q-factor of 20,000. They were able to detect an effective refractive index change of 10^{-7} RIU and had a detection limit of approximately 250 pg mm^{-2} mass coverage on the microring surface, which translated into ~160 fg of actual bound mass. In comparison with the interferometric devices presented above, the major advantage of ring-type devices is that because the light circulates within the ring each photon interacts with each bound molecule multiple times thereby potentially increasing the effective path length of the device.

As such while such devices may have similar sensitivity to bulk measures like mass per unit area, the actual required surface area is much smaller and thus the actual amount of mass required to impart a detectable signal is much smaller. This translates into a lower total mass LOD. In addition, it is relatively easy to multiplex such devices by placing rings of different sizes (and therefore exhibiting resonant peaks at different wavelengths) along a single bus waveguide.

16.2.3 Whispering Gallery Mode Devices

Operationally similar to ring resonators, microcavities sustaining whispering gallery modes (WGMs)[29,30] have recently been demonstrated for label-free biosensing. WGMs correspond to light being confined along a circular orbit along the edge of a sphere-, disk-, or cylinder-shaped structure. WGMs have been extensively studied in liquid droplets and fused silica spheres[31], both of which have nearly atomic scale smoothness. In such microcavities, optical losses are significantly lower than in other optical resonators and the Q-factor can exceed a hundred million. A number of variations on such devices have been demonstrated as biosensors for example that of Armani et al.[32] who demonstrated label-free biomolecular detection of a variety of different analytes with a solution phase LOD as low as 5 aM for Interleukin-2.

16.2.4 Planar Photonic Crystal-Based Biosensors

Photonic crystals[33] are composed of periodic dielectric structures. One of the features this periodicity gives rise to a range of wavelengths, which are not allowed to propagate within the structure, is referred to as the photonic bandgap. The size of the bandgap and its spectral position can be tuned by varying the refractive index contrast of the dielectric materials and/or the periodicity of the structure[34]. These properties of photonic crystals make them extremely useful in a number of applications, including biosensing. Of the different architectures that have been developed, high Q-factor 1D and 2D photonic-bandgap microcavity[35] sensors are particularly interesting as the probed volume is shrunk down to the size of the optical cavity, which can be on the order of λ^3. As alluded to above, since the mode volume is so small the total amount of mass required to result in a measurable change in the refractive index (similarly reflected by a change in the wavelength of the resonant peak) can also be very small. Examples of such systems include that of Lee et al.,[36] who demonstrated a 2D resonant photonic crystal-based biosensor for protein detection and Schmidt et al.,[22] who demonstrated a nanoparticle sensing in a unique 1D cavity. The drawback of these designs is that the large photonic bandgap prohibits having multiple sensing sites along the same waveguide. As such, the number of targets, which can be screened for at once, is relatively small. Ideally, one

would like an architecture that combines the high Q-factor and low mode volume sensing of the above devices with the ability to multiplex multiple detection sites along a single waveguide.

16.3 Our Approach to Improving on the State of the Art

There are numerous challenges involved in creating better biomolecular sensors, a number of which we have outlined in a recent review[15] and discussed throughout this book. Here we focus on how new device approaches can address the other emerging challenges such as the ability to simultaneously exhibit low LOD and high sensitivity, how to provide strong multiplexing capabilities, and how to simplify construction/assembly.

The technical challenge in addressing the former two of these is illustrated in Fig. 16.1. If we regard the goal of the sensor element itself as being able to provide as large of an output transduction signal as possible for the smallest amount of

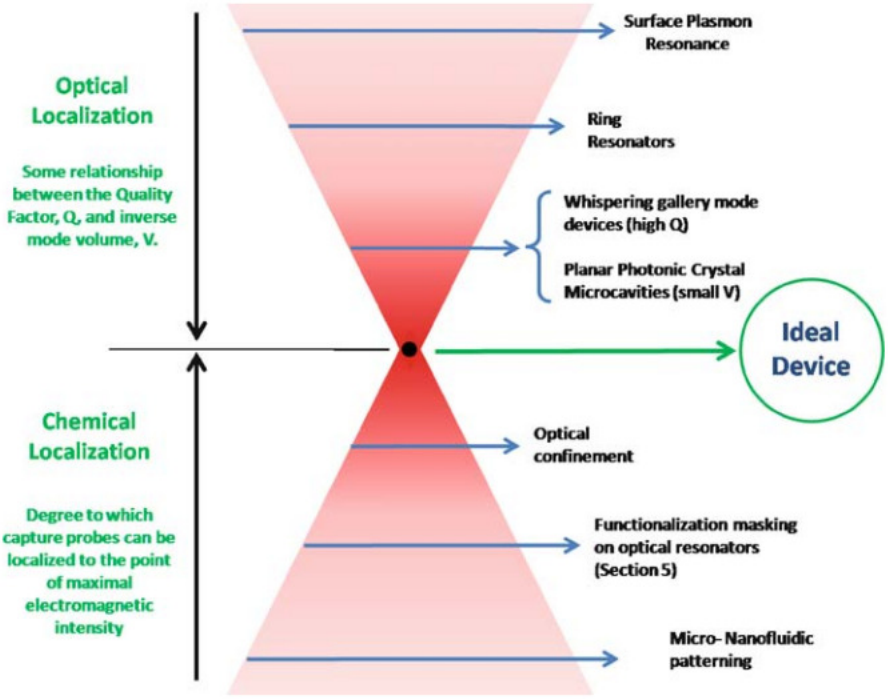

Fig. 16.1 Convergence of optical and chemical localization to improve biosensor performance. For label-free optical detection, ideally one would like to develop a system that maximizes the overlap between the optical localization (where the electromagnetic energy is concentrated) and the chemical localization (where the biomolecular target will be immobilized)

bound mass, it is clear that the optical sensor system must simultaneously confine the electromagnetic energy and the binding events to the same spatial location and that the energy density in this location should be as high as possible. Confining the electromagnetic energy down to a very small volume (such as in a photonic crystal microcavity) decreases the amount of functionalized area that is optically probed, but if the immobilization site is not also minimized, the same amount of mass is bound simply less of it is "seen." Therefore, without a chemical localization technique the improvement is likely to be marginal. We have placed broad groups of existing technologies at different locations along the axis in Fig. 16.1, to provide the reader with a general idea of how they might rank relative to each other. It is important to note, however, that because of the wide range of technologies within a particular subgroup, it is likely that different implementations could be at vastly different locations along these axes.

In the remaining two sections of this chapter, we discuss our efforts to address the challenges discussed above, through the development of an evanescently coupled linear optical resonator array architecture, which we have termed "Nanoscale Optofluidic Sensor Arrays." Section 16.4 outlines our technique for localizing electromagnetic energy in a device format that enables high quality factor, extreme multiplexibility, and relatively simplistic fabrication (approaching the apex in Fig. 16.1 from the top). Section 16.5 outlines our technique for spatial localization of the immobilization chemistry to ensure that the great majority of the binding events are "seen" by the sensor (approaching the apex in Fig. 16.2 from the bottom). Our goal given below will be to demonstrate the general design principles behind the approach and outlining how the techniques can be implemented on other designs. For further details, readers are referred to some of our recent papers namely Mandal and Erickson[37] and Goddard et al.[38]

16.4 Nanoscale Optofluidic Sensor Arrays

As mentioned above, the advantage of 1D photonic crystal cavities as biosensors is that they are likely the simplest possible optical devices able to concentrate electromagnetic energy down to spatial volumes as little as λ^3. The drawback of these designs is that the large photonic bandgap prohibits having multiple sensing sites along the same waveguide. Here we describe our technique for overcoming this limitation using evanescently coupled linear optical resonators. In the subsections below, we describe our approach, the fabrication and integration techniques used to construct the devices and some preliminary experimental/numerical results characterizing the technique. As will be demonstrated, this technique has a potential label-free LOD in the order of tens of attograms, while allowing for 2D multiplexing at reaction site densities at least equivalent to those found in a standard microarray.

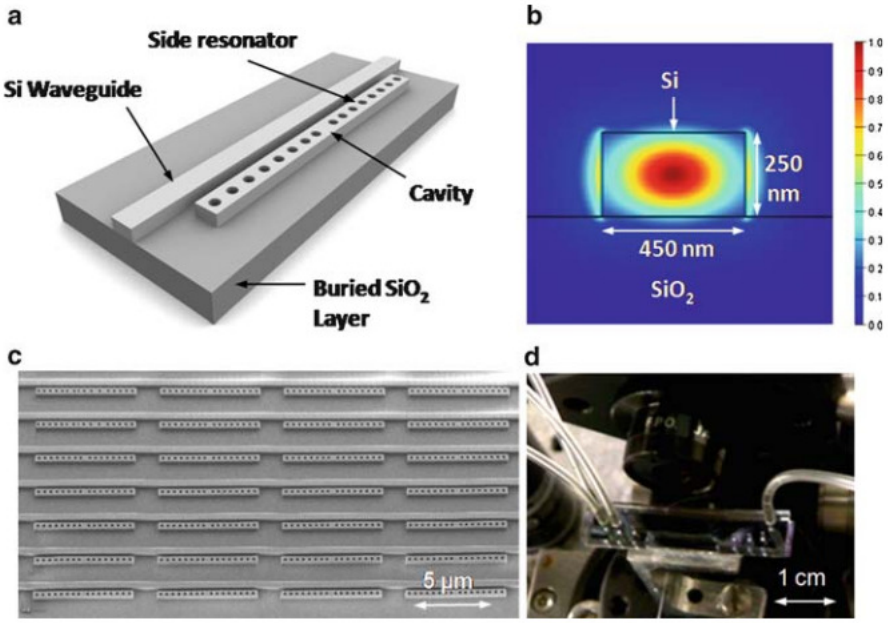

Fig. 16.2 Nanoscale optofluidic sensor arrays (NOSA). (**a**) 3D illustration of a NOSA sensing element. It consists of a 1D photonic crystal microcavity, which is evanescently coupled to a Si waveguide. (**b**) The electric field profile for the fundamental TE mode propagating through an air-clad Si waveguide on SiO_2. (**c**) SEM of a NOSA device array. It illustrates how this architecture is capable of two-dimensional multiplexing, thus affording a large degree of parallelism. (**d**) Actual NOSA chip with an aligned PDMS fluidic layer on top. Reprinted from Ref. 37 with permission. © 2008 Optical Society of America

16.4.1 Design Overview

Figure 16.2a shows a 3D illustration of our sensor design. It consists of a silicon (Si) waveguide with a 1D photonic crystal microcavity (side resonator) that lies adjacent to the waveguide. The side resonator consists of a central defect cavity with eight holes on either side, which forms the 1D photonic crystal. The Si waveguide was designed to be 450-nm wide and 250-nm tall to make it single mode. The low index silicon dioxide (SiO_2) layer which lies beneath the high index Si waveguide helps confine the light within the waveguide core, preventing optical losses into the lower substrate. Figure 16.2b shows the fundamental quasi-TE mode for this waveguide geometry.

A central defect cavity in the 1D photonic crystal gives rise to a defect state in the photonic bandgap. By varying this defect cavity spacing, we can tune the resonant wavelength of this state across the bandgap of the side resonator. Analogous to the ring resonators and WGM devices described above, light corresponding to the resonant wavelength couples evanescently into the side resonator and is sustained within it. This results in a dip in the output spectrum of the waveguide at

the resonant wavelength. Because the resonant structures lie to the side of the waveguide, the bandgap does not interfere with the light transmission outside of that which lies in the resonant peak. Thus our unique design allows multiplexing along a single waveguide by placement of a large number of side resonators along the waveguide, each of which is fabricated to have a slightly different resonant wavelength. Figure 16.2c shows an example 4 by 7 NOSA array and Fig. 16.2d shows the final device bonded to PDMS fluidics.

Figure 16.3 shows the steady-state electric field distribution in a given device (computed using 3D FDTD simulations) for both the (a) on resonance and (b) off resonance conditions. As can be seen, there is a significant amount of light amplification within the resonator. Relative to the evanescent field at the sidewalls and top of the resonator, we observe the inner most holes of the side resonator to have a stronger optical field. This causes the resonators to be very sensitive to refractive index changes within these holes due to the large degree of light–matter interaction inside them. Figure 16.3c demonstrates the typical output spectrum of a device with four evanescently coupled resonators (again computed using FDTD simulations). In this particular simulation, each resonator consists of four holes on either side of the central cavity as opposed to the eight shown in the above figures. The inherent advantage of our sensor design is apparent from this graph. By tuning the input light across a range of wavelengths and having a large number of side resonators (each designed to possess a unique resonant wavelength within this tunable range) placed alongside a single waveguide, the output spectrum will consist of a large number of sharp dips in an otherwise flat spectrum wherein each dip corresponds uniquely to one of the resonators. Any shift in one of the resonances indicates a change in the refractive index of the local environment

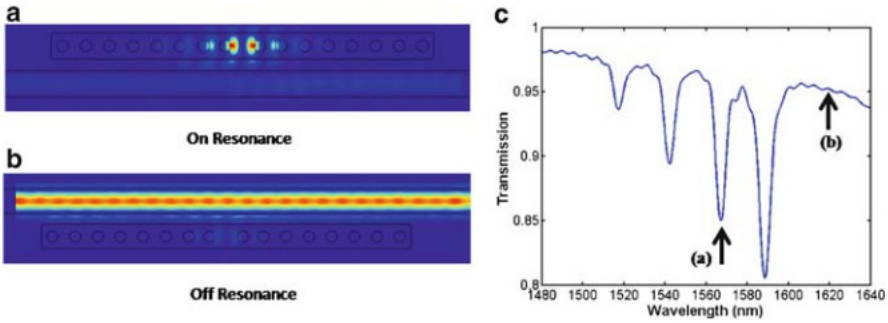

Fig. 16.3 Simulation of transmission spectrum for a four-resonator array. FDTD simulation showing the steady-state electric field distributions when the device is excited at the (**a**) resonant wavelength and (**b**) nonresonant wavelength. Note that the color levels in this image are scaled to the maximum field intensity in each image not to each other. The field levels in (**b**) are roughly of 20 times greater magnitude than those shown in (**a**). (**c**) Output spectrum for a device consisting of a waveguide with four evanescently coupled side cavities adjacent to it. Here each resonator consists of a cavity with four holes on either side. Reprinted from Ref. 37 with permission. © 2008 Optical Society of America

around the corresponding resonator. In this manner, a large number of detections can be done in parallel on a single waveguide.

16.4.2 Device Fabrication and System Integration

Figure 16.4 shows a schematic illustrating a version of the current fabrication method for our device. Briefly, the photonic devices were fabricated on SOI wafers having a device thickness of 250 nm. XR-1541 e-beam resist (HSQ, Dow-Corning Corporation) was spun on the wafer and the devices were patterned using a Leica VB6-HR electron beam lithography system. The Si device layer was then etched vertically down using a chlorine-based inductively coupled plasma etching system. The remaining XR-1541 was dissolved in a dilute 100:1 HF solution. To increase coupling efficiencies, nanotapers[39] were fabricated and a layer of hard baked SU-8 (Microchem) photoresist was used as a cladding to the nanotapers.

The top microfluidic architecture was fabricated using a multilayer soft lithography technique with polydimethylsiloxane (PDMS). In the figure, we illustrate a

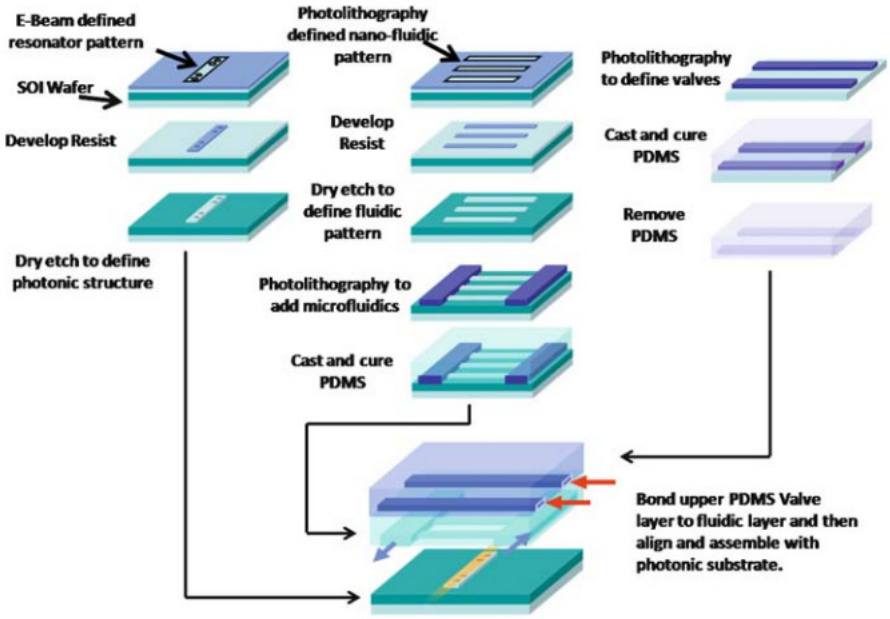

Fig. 16.4 Fabrication and assembly of the NOSA platform with PDMS microfluidics. The three elements of the fabrication are shown with the *left column* showing the steps involved in fabrication of the photonic structure, the *middle column* showing the fabrication of the fluidics, and the *right column* the fabrication of the valve layer. The *lower image* shows the assembly of the three elements into an integrated device similar to that shown in Fig. 16.2d

technique whereby nanofluidic channels are first defined in positive relief on an SOI wafer (analogous to how the photonic structures were fabricated) and then a microfluidic structure photolithographically patterned over them also in positive relief. In the majority of cases, however, the nanofluidic structures are not necessary and we forgo this step and simply pattern the microfluidics. In either case, liquid PDMS is spun coated over the fluidics layer and allowed to cure for approximately 90 min. Once cured the upper PDMS layer containing the pneumatic valves is bonded to the top side of the fluidic layer. To fabricate the complete device, the PDMS assembly was then aligned using a home-built rig and bonded reversibly to the chip. Precise alignment of the channels with the resonators during bonding was ensured by using a modified overhead optical microscope setup.

16.4.3 Experimental Demonstration

A typical, experimentally obtained, output spectrum of a waveguide with five resonators of differing sizes is shown in Fig. 16.5a. In this first case, all the five resonators had water as the surrounding medium. As can be seen, each resonator contributes a sharp dip to the output spectrum of the device. We observe that each 1D resonator possesses a large Q-factor varying from 1,500 to 3,000 and a full

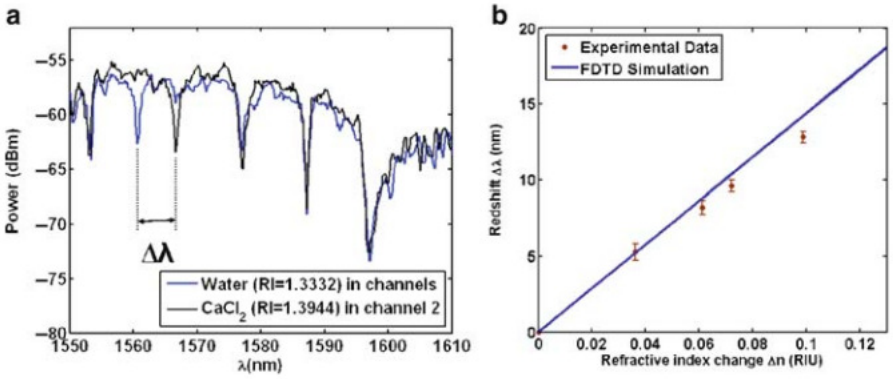

Fig. 16.5 Response to refractive index interrogation of a single NOSA waveguide. (**a**) Output spectrum for a NOSA where one of the five resonators is fluidically targeted, first with water and then with a $CaCl_2$ solution. The resonance of the targeted resonator shifts toward the red end of the spectrum due to the higher refractive index of the $CaCl_2$ solution. (**b**) Experimental data (with *error bars* indicating inter-device variability) showing the redshifts for various refractive index solutions. The *solid line* is the theoretically predicted redshift from FDTD simulations. The experimental data is in excellent agreement with the theory. Reprinted from Ref. 37 with permission. © 2008 Optical Society of America

width at half maxima of less than a nanometer. This is important for two reasons. First, higher Q-factors make it easier to detect very small shifts in the resonances. Equally as important, however, is that as the peaks get narrower it allows us to pack the output spectrum with a larger number of closely spaced dips and thus allows us to multiplex a larger number of resonators onto a single waveguide. Given the operational range of a standard 1,550-nm tunable laser (such as the one used here) and the linewidth of the observed resonances, we expect that 50 such side resonators could be incorporated on a single waveguide allowing us to perform as many as 50 detections in parallel on a single waveguide.

To investigate the refractive index sensitivity of the device we performed an experiment wherein one of the resonators was targeted by a fluidic channel, which was initially filled with water. When a higher refractive index solution of calcium chloride is passed through the channel, it changes the resonance condition of the resonator and pushes its unique resonant dip toward the red end of the spectrum as also shown in Fig. 16.5a. It is important to note that the other peaks are unaffected. In this way, one can confirm positive binding events occurring at any one of the resonators since only their corresponding resonances would show a shift in the output spectrum. Resonators with no binding occurring will show no shift in their output resonance.

The RI sensitivity of the NOSA devices was characterized by flowing fluids of different refractive indices through a channel targeting a particular resonator. We used deionized (DI) water as well as various concentrations of calcium chloride solution. The molar concentration of the $CaCl_2$ solutions varied from 1 to 5 M. The refractive indices of all the liquids were initially measured using a commercial refractometer. Figure 16.5b shows a plot of the shift in the resonant peak as a function of the change in refractive index of the fluid flowing through the channels. We observe an excellent match between the experimental data and the theoretically predicted redshifts. The slight discrepancy between the experimentally observed redshifts and those predicted by theory can possibly be attributed to optical losses in the waveguides and resonators arising due to surface roughness at their walls. The device exhibits a bulk refractive index sensitivity of over 130 nm for a unit shift in refractive index. Assuming a spectral resolution of 10 pm, we estimate the bulk refractive index detection limit of this device to be approximately 7×10^{-5}. Thus, while the refractive index LOD of this device is not as good as techniques like SPR, the ability to confine drastically the detection volume by targeting the holes allows us to lower the mass LOD.

16.4.4 Estimates of Device Performance

It is important to note that for applications such as biosensing, the device does not measure changes in the bulk refractive index of the surrounding medium, but rather respond to local changes in the refractive index at the surface of the sensor. As a result, the magnitude of the resonant shift will be dependent on a combination of

factors such as the biolayer thickness and the effective change in refractive index of the bound targets. To model this here, we performed detailed 3D FDTD simulations wherein we studied the sensitivity of this sensor design and determined how to achieve the lowest mass LOD using this architecture. We assumed that the resonator was initially functionalized by a 50-nm thick single-stranded DNA monolayer (ssDNA). When a detection event occurs, the complementary ssDNA strand of the target would hybridize with the functionalized capture probes forming double-stranded DNA (dsDNA). The ssDNA monolayer and the dsDNA monolayer were assumed to possess refractive indices of 1.456 and 1.53, respectively, and a binding density of 1.49 pmol cm^{-2}.[40] The molecular weight of the nucleic acids used in our simulations is 57,000 Da. We varied the number of holes being functionalized to study the mass sensitivity of the device as a function of the number of functionalized holes. Simulations were performed for the cases of two holes (the innermost holes on either side of the cavity), four holes (the inner two holes on either side), and so forth, up to 16 holes (eight holes on either side) being functionalized with an ssDNA capture probe. We have calculated the term $D\lambda/Dm$ in all these cases where $D\lambda$ is the shift in the resonant wavelength of the device caused due to positive binding events resulting in the formation of dsDNA and Dm is the mass of the bound target. This $D\lambda/Dm$ term is indicative of the mass sensitivity of the device. We use nucleic acids as are model species in this case due to the availability of data relating the change in local refractive index with surface concentration of immobilized probes and bound targets. For very large nucleic acid targets, however, there may be steric effects, which precludes transport into the resonator holes potentially

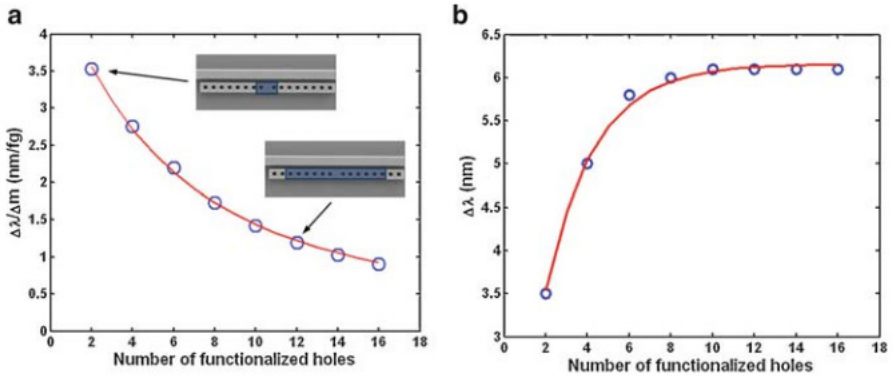

Fig. 16.6 Estimates of device performance in response to nucleic acid binding. (**a**) FDTD simulation showing the mass sensitivity of the device plotted as a function of the number of functionalized holes. The *circles* indicate the sensitivity values calculated from the simulations. The *solid curve* shows a least squares fit using an analytical model for the device sensitivity, which is described below. (**b**) Plot illustrating the dependence of the shift in resonant wavelength of a resonator on the number of functionalized holes. The *blue circles* indicate the data obtained from 3D FDTD simulations. The *solid curve* is a best-fit curve of the form $a(1-e^{-bN})$ where a and b are arbitrary constants. The values of a and b used here are 6.159 nm and 0.4273, respectively. Reprinted from Ref. 37 with permission. © 2008 Optical Society of America

degrading the overall sensitivity. For smaller nucleic acids or antibody/antigen systems we do not expect this to be a problem.

The circles in Fig. 16.6a show the calculated sensitivity, $\Delta\lambda/\Delta m$ for these different cases. As can be seen, the innermost holes are the most sensitive to any refractive index changes in the local environment as opposed to the holes that are further away from the cavity. These results can be explained by noting that the evanescent field is largest inside the innermost holes and decreases inside holes that are situated further away from the cavity. This is important to note because targeting only the inner most holes for functionalization allows for the lowest possible limit of mass detection for this device. In the case where only the inner two holes are functionalized we find that the resonance shifts by 3.5 nm when 1 fg of DNA binds to the resonator. Therefore, a mass change of 10 ag would result in a mass surface density of 0.84 ng cm^{-2} and an approximate shift of 0.01 nm, which can be experimentally detected. We therefore take this as the potential LOD of the device.

Figure 16.6b is a plot illustrating the dependence of the wavelength shift $\Delta\lambda$ on the number of functionalized holes N. We observe that an exponential function of the form $a(1-e^{-bN})$ (shown on the chart), where a and b are arbitrary constants that approximate this dependency quite well. To reiterate from above, although the resonant shift is larger for the greater number of holes, which are functionalized, more bound mass is required to impart this change. Thus increasing the number of holes, which are functionalized, tend to negatively affect the mass LOD.

16.5 Immobilization of Biological Recognition Elements Over Nanophotonic Biosensors

As alluded to above, as the design and fabrication of nanophotonic biosensors becomes more and more sophisticated, the difficulty in limiting immobilization of biomolecular recognition elements to the regions of highest optical intensity increases. Design of the optimal device requires maximal overlap between the concentrated electromagnetic energy and the biomolecular interaction to be detected. Binding events that occur outside this region of highest optical intensity are essentially lost (i.e., not detected by the device), negatively affecting the LOD of the device. An additional challenge is that as the probed area becomes smaller and optical intensity higher, the device is less able to average out surface heterogeneity and contaminants. Therefore, uniformity of immobilization chemistry and cleanliness of the final device are essential. In this section, we discuss our techniques for targeted immobilization of biomolecular capture probes over silicon nanophotonic devices. In targeting this chapter to the researcher more likely to be familiar with photonics than surface chemistry, we have focused here on providing practical advice on probe immobilization rather than detailed surface analysis. Readers interested in the latter should consult our recent paper[38].

16.5.1 Importance of Surface Cleanliness

In order to achieve uniform surface functionalization and subsequent biomolecule immobilization, the nanosensor surface must be free of any processing or environmental contaminants. Particular care must be taken when handling the finished devices, as well. Ungloved hands will of course contaminate the surface with various oils and salts, but even gloves can be a source of contamination, from the variety of oils and anticaking powders used to facilitate manufacturing of the gloves. The initial step in functionalizing the surface of a nanophotonic sensor often includes the generation of a silane monolayer. The stability of these monolayers depends on the uniform deposition of the silane and the ability of the silane molecules to cross-link with each other and with the hydroxylated surface. Surface contaminants will prevent the formation of well-defined monolayers. In addition, residues that interrupt the continuity of the cross-linked molecules allow moisture to penetrate the monolayer, resulting in hydrolysis of the siloxane bonds and loss of surface functionality.

Selection of an appropriate initial cleaning protocol will depend on the sensor substrate material. In the case of polymers, sonication in a range of solvents (in which the polymer is insoluble) followed by drying under nitrogen is often sufficient. For silicon-based nanosensors, a more thorough cleaning can be obtained by an ultraviolet (UV)/ozone treatment or oxygen plasma etching, both of which work by fragmenting the surface contaminants into lower molecular weight molecules that can be flushed away under vacuum or dissolved in solvents. In the case of plasma etching, it is important to remember that a dirty chamber often results in deposition of additional contaminants. A 10–20 min empty chamber etch is a prudent precleaning step. Wet chemical methods such as Piranha, MOS cleaning, and RCA cleaning methods provide even more aggressive cleaning. *Caution must be exercised when handling these wet chemical solutions, as many are strong bases, acids, or oxidizers, and can be explosive*. Analysis of the nanosensor surface following cleaning will ensure that the chosen cleaning protocol meets the needs of the device.

16.5.2 Biopatterning Techniques

For reasons described above, it is also critical that the patterning technique used to localize the biorecognition elements does not leave any residues. Microarray and inkjet printing are widely used biopatterning techniques, but their resolution is limited to a spot size between 10 and 100 mm. Additionally, the potential for capillary flow along topography makes these techniques less suitable for multiplexed optical nanostructures. Microcontact printing offers biopatterning on the scale of several micrometers, but the stamp can foul the surface, affecting device sensitivity[41–43]. Parylene biopatterning has proven to be an effective means to

immobilize biomolecules onto surfaces on the micrometer scale or smaller[44–47]. Unfortunately, it has been observed that a grassy parylene residue often remains on the substrate after standard lithography processing. This residue may be a result of contamination by metal particulates during the parylene deposition process and has been observed to be unaffected by longer etch times. Metal particulates embedded within the parylene thin film can form stable complexes with oxidized parylene[48], which are then resistant to complete etching. Because parylene is biocompatible, such residue may not pose an issue in applications such as fluorescence detection or cell patterning. However, in the development of optical nanosensors, surface contamination reduces signal intensity, which adversely impacts device sensitivity[49]. Therefore, when utilizing this technique for biopatterning onto optical nanostructures, it is necessary to ensure that the patterned substrate is free of any residues in order to maintain device sensitivity and high optical *Q*-factor.

A number of published reports investigating the long-term stability of parylene thin films have suggested that exposure to UV irradiation results in oxidative degradation[48,50,51]. On the basis of these reports, we have developed a simple method to eliminate the residues that often remain after standard parylene patterning, while retaining the bulk integrity of the patterned parylene film. In this technique, we demonstrate that UV irradiation followed by rinsing in an alkaline solution removes 98% of this parylene residue and demonstrated it on the device from Sect. 16.4. In order to prepare the surfaces for capture probe immobilization, sensor substrates were submerged in Piranha solution (3:1 mixture of concentrated sulfuric acid and 30% hydrogen peroxide) for 30 min, followed by rinsing in copious Milli-Q water in order to clean the surface and generate surface silanol (Si–OH) groups. A 1-mm film of Parylene C was vapor deposited onto clean silicon substrates, after which Microposit S1818 positive photoresist (Rohm and Haas, Marlborough, MA) was spun on to a thickness of approximately 2 mm. After exposure through a photomask and development of the exposed regions of the photoresist, the exposed parylene was etched in a Plasmatherm SLR-720 reactive ion etcher (30 sccm O_2, 60 mTorr, 150 W).

Grassy parylene residue was removed by exposing the etched substrates to 10 mW cm^{-2} UV irradiation at 254 nm for 1 min. The photooxidized residue product was then dissolved by rinsing the patterned nanosensor in deionized water adjusted to pH 12 by sodium hydroxide. Various irradiation and alkaline rinse conditions were tested from which it was determined that this combination provided the desired result without impacting the bulk parylene. Following UV/base treatment, substrates were rinsed in ethanol to remove residual photoresist. SEMs of control and UV/base-treated etched parylene substrates were taken to illustrate the effect of parylene residues on optical nanodevice performance, as well as the ability to target nucleic acid probes over the parallel 1D photonic crystal resonators, as shown in Fig. 16.7. Since nanometer-scale coatings have been reported to cause significant red-shifts in optical devices[52], device sensitivity will be affected by any residue. Our UV/base treatment effectively removed the residual parylene as shown in Fig. 16.7b. After UV/base treatment and immobilization of four nucleic acid probes

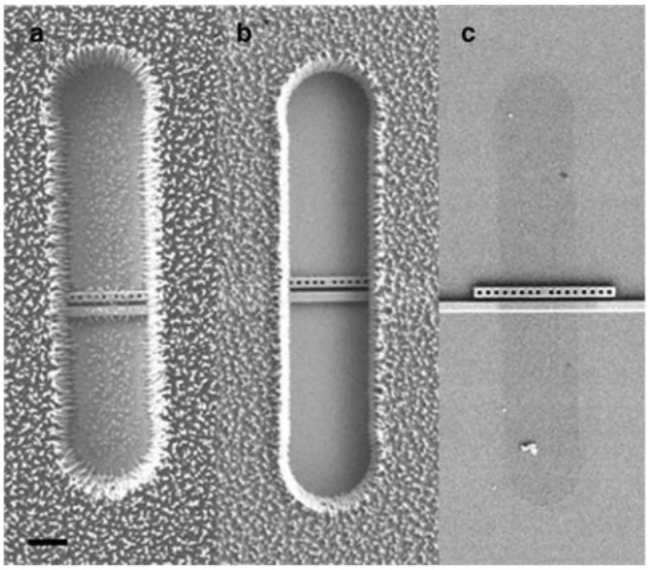

Fig. 16.7 SEM of parylene etched optical nanostructures (**a**) without UV/base treatment and (**b**) with UV/base treatment. (**c**) SEM image after removal of parylene. *Darkened spot* shows location of probes. Scale bar represents 2 m

over parallel resonators (details on probe immobilization follow), the parylene remained intact and was fully removed (Fig. 16.7c). Immobilized capture probes appear slightly darker due to differences in charging effects during SEM imaging between the biopatterned region and the unfunctionalized SiO_2 substrate. Again, for further details on the analysis, readers are referred to our recent paper[38].

16.5.3 Biopatterning for Multiplexed Detection

It is often desirable to immobilize different biomolecules on different sensing elements in close proximity on the same nanophotonic sensor in the development of a multiplexed sensor. This is the case in the example of parallel 1D photonic crystal resonators described in Sect. 16.4. Cross-contamination of biomolecules must be avoided in order to preserve high specificity. We have found that a combination of parylene biopatterning and polydimethylsiloxane (PDMS) microfluidics is a convenient means to immobilized multiple biomolecules in close proximity without cross-contamination as shown in Fig. 16.8. Parylene biopatterning is first used to expose only the regions of highest optical intensity of the nanosensor for functionalization. Second, a set of PDMS microfluidics is applied to the parylene-patterned nanophotonic sensor, and the biomolecules to be attached

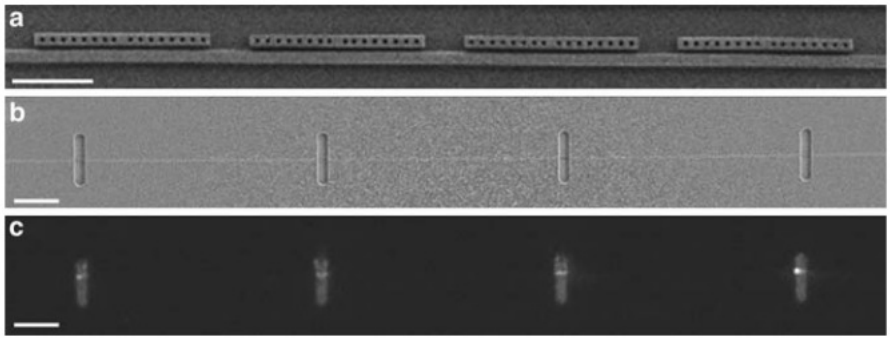

Fig. 16.8 Multiplexing immobilization on paralell resonators. (**a**) SEM of parallel resonators (scale bar is 3 mm). (**b**) SEM of parallel parylene patterned 1D photonic crystal resonators (scale bar is 20 mm). (**c**) Fluorescence micrograph of patterned capture probes after parylene removal (scale bar is 20 mm)

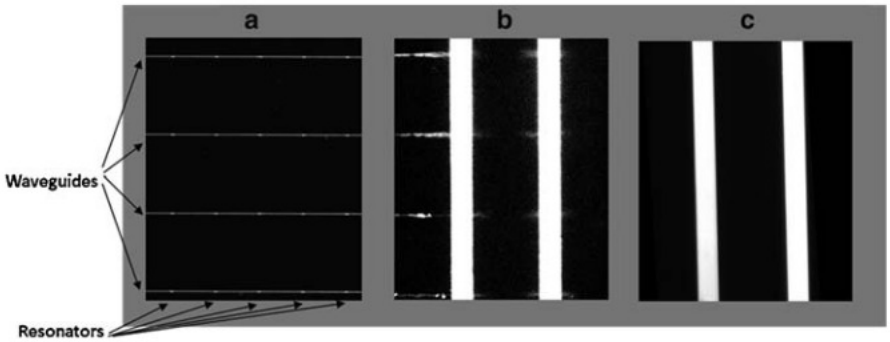

Fig. 16.9 Micrographs illustrating microfluidic targeting over structured substrate. (**a**) Optical micrograph of optical nanostructure. (**b**) Without parylene patterning, fluidic channels leak along waveguides within 5 min. (**c**) With parylene patterning, channels maintain integrity for full hour

are drawn through the microfluidic channel. In using this combined technique, we have observed an additional benefit to using parylene biopatterning over topographical substrates such as our photonic crystal resonators and waveguides. Although parylene deposition is reported to be a conformal coating, it provides sufficient planarization to prevent leaking during fluidic targeting of biomolecules over structured nanodevices. Figure 16.9 illustrates the fluidic integrity of structured nanodevices with, Fig. 16.9c, and without parylene, Fig. 16.9b. In both images, alternating channels of fluorescein isothiocyanate in water and water alone were withdrawn for 60 min across a nanostructured optical device. Leaking was evident on the uncoated substrates after less than 5 min; whereas parylene-coated devices exhibited no leakage through the course of the study.

16.5.4 Chemistry of Biomolecular Immobilization

In addition to selecting an appropriate biopatterning technique, consideration must be given to the method of immobilizing the biorecognition element. The major methods of immobilizing biological recognition elements include adsorption, electrostatic interactions, ligand/receptor pairing, and covalent binding. Adsorption is the simplest, and is suitable for single-use devices; however, it provides no specificity with regards to biomolecule orientation, and it is unlikely to withstand rigorous rinse steps. Electrostatic interactions can be long lasting, provided the pH and ionic strength of the sensor environment remains within the appropriate isoelectric points of the biomolecule and substrate. Ligand receptor pairing, such as the biotin–streptavidin interaction, provides the strongest noncovalent bond. The commercial availability of numerous biotinylated bioconjugation reagents (antibodies, oligonucleotides, enzymes, etc.) has made this method of immobilization a convenient option. A covalent bond provides the strongest linkage between the biomolecule and the substrate, and provides the greatest potential for a reusable device. By targeting specific reactive functional groups on both the biomolecule and the substrate, one is also better able to control the orientation of the immobilized biomolecule. This is of particular importance in the case of antibodies and oligonucleotides, in which proper orientation greatly impacts analyte binding efficiency.

As mentioned previously, the initial step in functionalization is often achieved by use of a silane cross-linker. Use of a mixed monolayer, in which multiple silane components are cross-linked together to form the silane monolayer, may help space out the reactive functional groups to prevent overcrowding of biorecognition elements, which adversely affects analyte binding efficiency. Silane monolayers can be formed by submersion in a solution of silane in organic solvent or by vapor phase deposition. Exposure to water must be carefully controlled to prevent polymerization of the silane and formation of multilayers. The deposited monolayer should be allowed to cure (overnight at room temperature or 1–2 h at 60–80°C is sufficient) to allow formation of siloxane cross-links. Biological recognition elements can then be directly linked to the nanophotonic sensor substrate by conjugation to the silane's terminal functionality; however, it is often beneficial to link the biomolecule via a tether molecule. Tether molecules such as poly(ethylene glycol) reagents and dendrimers can improve analyte binding efficiency by shielding the biomolecule from adverse surface-induced effects and by lessening steric hindrance[53–56]. Poly(ethylene glycol) offers additional advantages by reducing nonspecific adsorption of nontarget molecules within the sample matrix[57] and, in the case of sensors that incorporate micro- or nanofluidics, by providing a hydrophilic surface that improves fluid flow. Another consideration in selecting an appropriate functionalization chemistry is that in order to avoid high background signal from nonspecific adsorption, there should be little affinity between the target analyte and the tether molecule.

16.5.5 A Brief Practical Example for the Immobilization of Nucleic Acid Probes

To close off this section, we will briefly overview a surface functionalization chemistry scheme we have developed for immobilization of four separate nucleic acid capture probes over our NOSA resonators described in Sect. 16.4. The goal of this technique is to maximize hybridization efficiency while minimizing nonspecific adsorption of noncomplementary target. This is achieved by using carboxylic acid terminated generation 4.5 dendrimers (Dendritech, Inc., Midland, MI) as a tether molecule. Figure 16.10 illustrates the overall reaction scheme for immobilization of DNA capture probes onto patterned SiO_2 substrates. We have used this functionalization chemistry in combination with the residue-free parylene biopatterning and microfluidic targeting techniques described previously to limit the immobilization of fluorescently tagged nucleic acid capture probes over the regions of highest optical intensity within 1D photonic crystals, as described above. Utilizing carboxy-terminated dendrimers to tether nucleic acid capture probes to surfaces offers several advantages. Their branched, semispherical structure distances the immobilized capture probes from the solid surface, thus improving immobilization density and hybridization yields when used as a linker molecule[53–56,58]. When the dendritic linker is carboxyterminated, electrostatic interactions between target analyte and silicon substrate are minimized, thus reducing nonspecific binding vs. the more commonly used amine-terminated PAMAM dendrimer. We thus designed our surface functionalization chemistry to take advantage of these unique properties, while also limiting the overall height of the biopatterned region to the region of highest optical intensity within the evanescent field of the resonators.

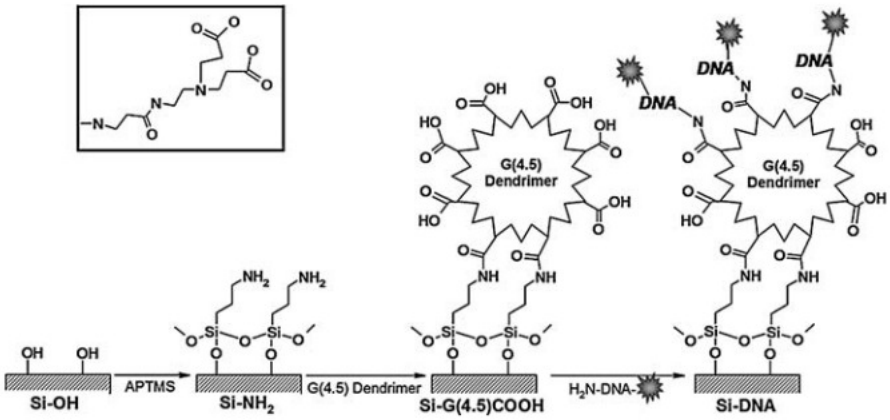

Fig. 16.10 Reaction scheme for immobilization of DNA onto functionalized SiO_2 substrates. Plasma-treated SiO_2 substrates are denoted as Si-OH, APTMS functionalized substrates are denoted as Si-NH_2, dendrimer functionalized substrates are denoted as Si-G(4.5)COOH, and substrates to which DNA capture probes have been immobilized are denoted as Si-DNA. *Inset*: Repeat unit of PAMAM dendrimer possessing terminal carboxylic acid functionality

Following parylene patterning and UV/base treatment as described above, patterned substrates were shaken in a solution of aminopropyltrimethoxysilane (APTMS, TCI America, Portland, OR) in ethanol for 5 min, followed by ethanol and water rinses, and curing for 1 h at 80°C. Generation 4.5 carboxylic acid-terminated dendrimers were covalently linked to the amine-functionalized substrates using water soluble carbodiimide chemistry[59]. Substrates were shaken for 2 h at room temperature in a solution of 10 mM dendrimer in 0.067 M phosphate buffer, pH 7.4, containing EDC and NHS, followed by rinsing in deionized water and drying under air. Subsequently, amine-terminated DNA capture probes (Operon Biotechnologies, Huntsville, AL) were bound to the carboxyl-functionalized SiO_2 surfaces via two-step water-soluble carbodiimide chemistry[59]. Briefly, surfaces were first shaken for 15 min in 0.1 M MES buffer, pH 6, containing EDC and NHS, followed by rinsing in water and drying under air. In order to separately address parallel resonators such that a different capture probe could be immobilized on each resonator, a PDMS microfluidics were applied to the substrate as described above. Amine-terminated DNA probes were diluted to 150 mM in 0.1 M MES buffer, pH 5.0 (final conjugation buffer was pH 7.0). Probes were withdrawn through microchannels for 2 h at room temperature, followed by in-channel water rinsing. Nucleic acid functionalized substrates (Si-DNA) were then removed from the plexiglass housing, PDMS microchannels and parylene film were peeled off the substrate, and the substrate was rinsed in deionized water and air dried.

16.6 Summary

In this chapter, we have attempted to describe broadly the advantages available from the use of planar nanophotonic devices as biomolecular detectors. We have reviewed the state of the art in these devices and described a few technical challenges involved in improving these devices. In the context of these challenges, we have introduced our "Nanoscale Optofluidic Sensor Arrays" which represents our attempt to address them.

References

1 Rich, R. L.; Myszka, D. G., Survey of the year 2006 commercial optical biosensor literature, *J. Mol. Recognit.* **2007**, 20, 300–366
2 Sander, C., Genomic medicine and the future of health care, *Science* **2000**, 287, 1977–1978
3 Srinivas, P. R.; Kramer, B. S.; Srivastava, S., Trends in biomarker research for cancer detection, *Lancet Oncol.* **2001**, 2, 698–704
4 Srinivas, P. R.; Verma, M.; Zhao, Y. M.; Srivastava, S., Proteomics for cancer biomarker discovery, *Clin. Chem.* **2002**, 48, 1160–1169
5 Growdon, J. H., Biomarkers of Alzheimer disease, *Arch. Neurol.* **1999**, 56, 281–283

6 Ross, J. S.; Schenkein, D. P.; Kashala, O.; Linette, G. P.; Stec, J.; Symmans, W. F.; Pusztai, L.; Hortobagyi, G. N., Pharmacogenomics, *Adv. Anat. Pathol.* **2004**, 11, 211–220

7 Hernandez, J.; Thompson, I. M., Prostate-specific antigen: A review of the validation of the most commonly used cancer biomarker, *Cancer* **2004**, 101, 894–904

8 Ward, A. M.; Catto, J. W. F.; Hamdy, F. C., Prostate specific antigen: Biology, biochemistry and available commercial assays, *Ann. Clin. Biochem.* **2001**, 38, 633–651

9 Sidransky, D., Emerging molecular markers of cancer, *Nat. Rev. Cancer* **2002**, 2, 210–219

10 Wulfkuhle, J. D.; Liotta, L. A.; Petricoin, E. F., Proteomic applications for the early detection of cancer, *Nat. Rev. Cancer* **2003**, 3, 267–275

11 Straub, T. M.; Chandler, D. P., Towards a unified system for detecting waterborne pathogens, *J. Microbiol. Methods* **2003**, 53, 185–197

12 Rasooly, A.; Herold, K. E., Biosensors for the analysis of food- and waterborne pathogens and their toxins, *J. AOAC Int.* **2006**, 89, 873–883

13 McBride, M. T.; Masquelier, D.; Hindson, B. J.; Makarewicz, A. J.; Brown, S.; Burris, K.; Metz, T.; Langlois, R. G.; Tsang, K. W.; Bryan, R.; Anderson, D. A.; Venkateswaran, K. S.; Milanovich, F. P.; Colston, B. W., Autonomous detection of aerosolized *Bacillus anthracis* and *Yersinia pestis*, *Anal. Chem.* **2003**, 75, 5293–5299

14 Stetzenbach, L. D.; Buttner, M. P.; Cruz, P., Detection and enumeration of airborne biocontaminants, *Curr. Opin. Biotechnol.* **2004**, 15, 170–174

15 Erickson, D.; Mandal, S.; Yang, A.; Cordovez, B., Nanobiosensors: Optofluidic, electrical and mechanical approaches to biomolecular detection at the nanoscale, *Microfluid. Nanofluid.* **2008**, 4, 33–52

16 Seydack, M., Nanoparticle labels in immunosensing using optical detection methods, *Biosensors Bioelectron.* **2005**, 20, 2454–2469

17 Zheng, G. F.; Patolsky, F.; Cui, Y.; Wang, W. U.; Lieber, C. M., Multiplexed electrical detection of cancer markers with nanowire sensor arrays, *Nat. Biotechnol.* **2005**, 23, 1294–1301

18 Li, C.; Curreli, M.; Lin, H.; Lei, B.; Ishikawa, F. N.; Datar, R.; Cote, R. J.; Thompson, M. E.; Zhou, C. W., Complementary detection of prostate-specific antigen using ln(2)O(3) nanowires and carbon nanotubes, *J. Am. Chem. Soc.* **2005**, 127, 12484–12485

19 Majumdar, A., Bioassays based on molecular nanomechanics, *Dis. Markers* **2002**, 18, 167–174

20 Ouyang, H.; Striemer, C. C.; Fauchet, P. M., Quantitative analysis of the sensitivity of porous silicon optical biosensors, *Appl. Phys. Lett.* **2006**, 88, 163108

21 Chow, E.; Grot, A.; Mirkarimi, L. W.; Sigalas, M.; Girolami, G., Ultracompact biochemical sensor built with two-dimensional photonic crystal microcavity, *Opt. Lett.* **2004**, 29, 1093–1095

22 Schmidt, B.; Almeida, V.; Manolatou, C.; Preble, S.; Lipson, M., Nanocavity in a silicon waveguide for ultrasensitive nanoparticle detection, *Appl. Phys. Lett.* **2004**, 85, 4854–4856

23 Pollock, C.; Lipson, M., Integrated Photonics, Kluwer, Norwell, MA, **2003**.

24 Prasad, P., Nanophotonics, Wiley, Hoboken, NJ, **2004**.

25 Luff, B. J.; Wilkinson, J. S.; Piehler, J.; Hollenbach, U.; Ingenhoff, J.; Fabricius, N., Integrated optical Mach-Zehnder biosensor, *J. Lightwave Technol.* **1998**, 16, 583–592

26 Prieto, F.; Sepulveda, B.; Calle, A.; Llobera, A.; Dominguez, C.; Abad, A.; Montoya, A.; Lechuga, L. M., An integrated optical interferometric nanodevice based on silicon technology for biosensor applications, *Nanotechnology* **2003**, 14, 907–912

27 Heideman, R. G.; Lambeck, P. V., Remote opto-chemical sensing with extreme sensitivity: Design, fabrication and performance of a pigtailed integrated optical phase-modulated Mach-Zehnder interferometer system, *Sensors Actuat. B-Chem.* **1999**, 61, 100–127

28 Chao, C. Y.; Fung, W.; Guo, L. J., Polymer microring resonators for biochemical sensing applications, *IEEE J. Sel. Top. Quantum Electron.* **2006**, 12, 134–142

29 Matsko, A. B.; Ilchenko, V. S., Optical resonators with whispering-gallery modes – Part I: Basics, *IEEE J. Sel. Top. Quantum Electron.* **2006**, 12, 3–14

30 Ilchenko, V. S.; Matsko, A. B., Optical resonators with whispering-gallery modes – Part II: Applications, *IEEE J. Sel. Top. Quantum Electron.* **2006**, 12, 15–32
31 Arnold, S.; Khoshsima, M.; Teraoka, I.; Holler, S.; Vollmer, F., Shift of whispering-gallery modes in microspheres by protein adsorption, *Opt. Lett.* **2003**, 28, 272–274
32 Armani, A. M.; Kulkarni, R. P.; Fraser, S. E.; Flagan, R. C.; Vahala, K. J., Label-free, single-molecule detection with optical microcavities, *Science* **2007**, 317, 783–787
33 Joannopoulos, J. D.; Meade, R. D.; Winn, J. W., Photonic Crystals: Molding the Flow of Light, Princeton University Press, Princeton, NJ, 1995
34 Erickson, D.; Rockwood, T.; Emery, T.; Scherer, A.; Psaltis, D., Nanofluidic tuning of photonic crystal circuits, *Opt. Lett.* **2006**, 31, 59–61
35 Foresi, J. S.; Villeneuve, P. R.; Ferrera, J.; Thoen, E. R.; Steinmeyer, G.; Fan, S.; Joannopoulos, J. D.; Kimerling, L. C.; Smith, H. I.; Ippen, E. P., Photonic-bandgap microcavities in optical waveguides, *Nature* **1997**, 390, 143–145
36 Lee, M. R.; Fauchet, P. M., Two-dimensional silicon photonic crystal based biosensing platform for protein detection, *Opt. Express* **2007**, 15, 4530–4535
37 Mandal, S.; Erickson, D., Nanoscale optofluidic sensor arrays, *Opt. Express* **2008**, 16, 1623–1631
38 Goddard, J.; Erickson, D.; "Bioconjugation Techniques for Microfluidic Biosensors" *Analytical and Bioanalytical Chemistry* **2009**, 394, 469–479
39 Almeida, V. R.; Panepucci, R. R.; Lipson, M., Nanotaper for compact mode conversion, *Opt. Lett.* **2003**, 28, 1302–1304
40 Elhadj, S.; Singh, G.; Saraf, R. F., Optical properties of an immobilized DNA monolayer from 255 to 700 nm, *Langmuir* **2004**, 20, 5539–5543
41 Barbulovic–Nad, I.; Lucente, M.; Sun, Y.; Zhang, M. J.; Wheeler, A. R.; Bussmann, M., Bio-microarray fabrication techniques - A review, *Crit. Rev. Biotechnol.* **2006**, 26, 237–259
42 Xu, L. P.; Robert, L.; Qi, O. Y.; Taddei, F.; Chen, Y.; Lindner, A. B.; Baigl, D., Microcontact printing of living bacteria arrays with cellular resolution, *Nano Lett.* **2007**, 7, 2068–2072
43 Mannini, M.; Bonacchi, D.; Zobbi, L.; Piras, F. M.; Speets, E. A.; Caneschi, A.; Cornia, A.; Magnani, A.; Ravoo, B. J.; Reinhoudt, D. N.; Sessoli, R.; Gatteschi, D., Advances in single-molecule magnet surface patterning through microcontact printing, *Nano Lett.* **2005**, 5, 1435–1438
44 Ilic, B.; Craighead, H. G., Topographical patterning of chemically sensitive biological materials using a polymer-based dry lift off, *Biomed. Microdevices* **2000**, 2, 317–322
45 Moran-Mirabal, J.; Tan, C.; Orth, R.; Williams, E.; Craighead, H.; Lin, D., Controlling microarray spot morphology with polymer liftoff arrays, *Anal. Chem.* **2007**, 79, 1109–1114
46 Orth, R. N.; Kameoka, J.; Zipfel, W. R.; Ilic, B.; Webb, W. W.; Clark, T. G.; Craighead, H. G., Creating biological membranes on the micron scale: Forming patterned lipid bilayers using a polymer lift-off technique, *Biophys. J.* **2003**, 85, 3066–3073
47 Atsuta, K.; Suzuki, H.; Takeuchi, S., A parylene lift-off process with microfluidic channels for selective protein patterning, *J. Micromech. Microeng.* **2007**, 17, 496–500
48 Majid, N.; Dabral, S.; McDonald, J. F., The parylene-aluminum multilayer interconnection system for wafer scale integration and wafer scale hybrid packaging, *J. Electron. Mater.* **1989**, 18, 301–311
49 Byun, K. M.; Yoon, S. J.; Kim, D.; Kim, S. J., Sensitivity analysis of a nanowire-based surface plasmon resonance biosensor in the presence of surface roughness, *J. Opt. Soc. Am. A: Opt. Image Sci. Vis.* **2007**, 24, 522–529
50 Fortin, J. B.; Lu, T. M., Ultraviolet radiation induced degradation of poly-*para*-xylylene (parylene) thin films, *Thin Solid Films* **2001**, 397, 223–228
51 Pruden, K. G.; Sinclair, K.; Beaudoin, S., Characterization of parylene-N and parylene-C photooxidation, *J. Polym. Sci. Part A: Polym. Chem.* **2003**, 41, 1486–1496
52 Lee, M.; Fauchet, P. M., Two-dimensional silicon photonic crystal based biosensing platform for protein detection, *Opt. Express* **2007**, 15, 4530–4535

53 Le Berre, V.; Trevisiol, E.; Dagkessamanskaia, A.; Sokol, S.; Caminade, A. M.; Majoral, J. P.; Meunier, B.; Francois, J., Dendrimeric coating of glass slides for sensitive DNA microarrays analysis, *Nucleic Acids Res.* **2003**, 31, e88
54 Pathak, S.; Singh, A. K.; McElhanon, J. R.; Dentinger, P. M., Dendrimer-activated surfaces for high density and high activity protein chip applications, *Langmuir* **2004**, 20, 6075–6079
55 Benters, R.; Niemeyer, C. M.; Wohrle, D., Dendrimer-activated-solid supports for nucleic acid and protein microarrays, *Chembiochem.* **2001**, 2, 686–694
56 Benters, R.; Niemeyer, C. M.; Drutschmann, D.; Blohm, D.; Wohrle, D., DNA microarrays with PAMAM dendritic linker systems, *Nucleic Acids Res.* **2002**, 30, e10
57 Harris, J. M., Poly(Ethyelene Glycol) Chemistry: Biotechnical and Biomedical Applications, Plenum, New York, NY, **1992**, 385
58 Caminade, A. M.; Padie, C.; Laurent, R.; Maraval, A.; Majoral, J. P., Uses of dendrimers for DNA microarrays, *Sensors* **2006**, 6, 901–914
59 Hermanson, G. T., Bioconjugate Techniques, Academic, New York, NY, **1996**, 785